Stagnation-Point Ablation of Carbonaceous Flat Disks—Part I: Theory

Chul Park*
NASA Ames Research Center, Moffett, Field, California

The process of ablation is calculated for the stagnation region of a flat disk in a radiation-dominated, massive-blowing environment produced in a ballistic range filled with argon. Flow environments are determined by solving the boundary-layer equations while radiative transfer is calculated through a line-by-line spectral computation. The resulting wall heat-transfer rates are coupled with an existing material's response code to determine surface recession and char thickness. The calculation is performed for six 5-cm-diam models made of carbon-phenolic and carbon-carbon composite launched in the Track-G facility at the Arnold Engineering Development Center. Significant surface recessions are predicted to occur for these models due mostly to radiative heating.

Nomenclature

a_1-a_3 = constants in ϕ, Eq. (2)
C = mean molecular speed = $(8kT/\pi m)^{1/2}$
C_h = mass-transfer coefficient
C_p = specific heat at constant pressure
e = emissivity
f = dimensionless velocity function in boundary-layer coordinate
h_v = vaporization energy
k = Boltzmann constant
K = thermal conductivity
m = mean molecular mass
$\dot{m}$ = mass-loss rate (ablation rate)
p = pressure
q = heat flux
R_n = equivalent sphere radius
Re_∞ = freestream Reynolds number = $\rho_\infty v_\infty R_n/\mu_\infty$
t = time
T = temperature
v = velocity normal to wall
V = recession velocity
y = distance normal to wall
α = ablation-product mass fraction
β = vaporization coefficient
γ = adiabatic exponent
δ = recession
Δ = char thickness
μ = viscosity
ρ = density
σ = Stefan-Boltzmann constant
ϕ = radiative blockage factor, Eq. (1)
Φ = parameter defined by Eq. (4)

Subscripts

a = absorbed
A = inviscid argon shock layer
c = convective
e = edge of ablation layer
E = equilibrium
m = solid material
r = radiative
s = stagnation region
w = wall
∞ = freestream

Received May 28, 1982; revision received Jan. 3, 1983. This paper is declared a work of the U.S. Government and therefore is in the public domain.

*Research Scientist, Entry Technology Branch. Member AIAA.

Introduction

WHEN a blunt body travels at a high speed through the atmosphere of a planet, its shock layer can reach high enough temperatures to emit strong radiation. A combination of high radiative heat flux and a large flow Reynolds number produces a condition described as a massive-blowing environment.[1] In this environment, a thick layer of ablation-product gas, referred to as a blowing layer, or ablation layer, develops over the heat-shield wall surface. The radiative heat flux emitted by the shock layer is partly absorbed by this layer, and hence the ablation rate is affected by its opacity.

The massive-blowing condition occurs typically in entry flights into the outer planets,[2] or in flights through the Earth's atmosphere at superorbital speeds.[3] For such flight regimes, reflective heat shields, made of silica, and absorptive heat shields, made of carbonaceous materials, such as graphite, carbon-phenolic, or carbon-carbon composite, have been developed.[4] Although extensive calculations have been made to predict the ablative performance of these heat-shield materials,[5] the accuracy of the calculations has not yet been fully verified. To verify the accuracy, it is necessary to experimentally test the heat-shield material in a radiation-dominated, massive-blowing environment.

Experimentally, heat-shield materials have been tested in arc-heated wind tunnels and with gasdynamic lasers.[5] These facilities produce useful levels of radiative heat fluxes but fail to meet other requirements: arc-heated wind tunnels do not produce flow Reynolds numbers high enough to induce a massive-blowing environment, and the laser fails to simulate either the radiation spectra or the hypersonic boundary-layer phenomenon. One known means of testing ablative characteristics under high heat-transfer rates is a ballistic range facility. In such a facility, convective heat-transfer rates of the order of 100 kW/cm^2 are produced by using air as the test gas.[6-8] A radiative environment can be produced by using argon as the test gas instead of air. In an argon environment, a flight velocity of 5 km/s attainable in such a facility produces a shock-layer temperature of about 15,000 K (Ref. 9). As a result, radiative heat fluxes of the order of 100 kW/cm^2 are predicted to be produced at the nose region of a model with a radius of the order of 1 cm (Ref. 9). Spectra of argon roughly resemble those of the common gases in the giant planets, and hence the optical aspect of the problem is simulated.[9]

The purpose of the present two-part work is to study the ablation characteristics of carbonaceous heat-shield materials experimentally in a radiation-dominated, massive-blowing environment, and to compare the results with the best available theoretical predictions. For this purpose, six flat-

disk models (5 cm diameter), two made of carbon-carbon and four made of carbon-phenolic, were launched in a track-range facility[6-8] filled with argon. Wall radiative heat fluxes in the range of tens of kW/cm^2 and Reynolds numbers of the order of 10^6 are produced by this means, leading to a massive-blowing environment. This first part of the work describes the theoretical methods of prediction and the results of the calculations; the second part describes the experiment and compares the theoretical predictions with the experimental results.[10]

At several locations along the track, head-on image-converter photographs are taken of the traveling models in order to determine the surface temperature, surface topography, and the extent of spallation. To avoid viewing the surface through a luminous shock layer, the region is flushed with helium,[6-8] which produces a shock temperature of about 3000 K. While the model passes through this region, a nearly explosive ablation occurs by the process to be described in detail later. This near-explosion phenomenon must be accounted for in order to properly interpret the image-converter photographs.

In principle, the ablation behavior at the stagnation region of the models should be calculable by running an existing flowfield environmental code accounting for radiation, such as radiating shock layer environment (RASLE),[11] simultaneously with a materials response code, such as charring materials ablation (CMA).[12] In practice, such a computation would be prohibitively time consuming and expensive. Furthermore, existing materials' response codes cannot accommodate the nearly explosive phenomenon in the helium environment.

In the present paper, two separate approaches are taken in order to address these two problems. First, to determine surface recessions, the flow environments are calculated using a boundary-layer approach. The computing time is much shorter with the boundary-layer approach than with the viscous shock-layer method used in the existing more general environmental codes.[5,11] By selecting the Prandtl and Schmidt numbers appropriately, the present work shows that the boundary-layer method reproduces the results of a viscous shock-layer calculation[11] for the environment of concern. The radiative heat fluxes emanating from the inviscid region of the shock layer, and their transmission through the boundary layer, are calculated in more detail than in the existing environmental code[11] using a line-by-line spectral computation method.[13] The calculated wall heat-transfer rates are directly coupled with the CMA code to calculate the pyrolysis and ablation phenomena. The nearly explosive mass-transfer phenomenon is neglected for the CMA calculation. The calculation yields surface recession and, in the case of carbon-phenolic models, char thicknesses, both of which are compared with the experimental data in Part II.

Second, in order to interpret the image-converter photographs, a code, identified as stagnation point ablation in flight test (SPAIFT), is developed. This code carries out a time integration of heat- and mass-transfer processes in a manner similar to the first method, but it accommodates the nearly explosive phenomenon in the helium environment. The code neglects the pyrolysis phenomenon within the material, and hence errs slightly in recession prediction, but it produces correct results for the surface temperature while the model is in the helium environment. The results of this calculation will be compared with experimental data in Part II also.

Method of Calculation

Test Environments

In a track-range facility, the launched models travel ballistically, confined by four steel tracks.[6] The track used in the present tests (at the Arnold Engineering Development Center)[6] passes through a blast tank filled with helium, through an uprange that is 93 m long, and through a downrange that is 174 m long. In the present work, the two ranges are filled with argon to the same pressure. The downstream end of the range is connected to the recovery tube in which the model is stopped by high-pressure nitrogen.

The launch conditions of the present tests are listed in Table 1. The models for shots 5591 and 5605 were made of multidimensional carbon-carbon composite (CC). The models for shots 5599, 5601, and 5602 were made of chop-molded carbon-phenolic (CMCP). The model for shot 5604 was made with inverted-chevron carbon-phenolic (ICCP). The models are initially at room temperature. Of the six models launched, five were recovered. One, shot 5602, was destroyed during the recovery process. The models had an initial overall radius of 2.54 cm.

Laser shadowgraphs are taken at seven stations along the range for flow visualization. Head-on image-converter (imacon) pyrometric photographs of the models are taken at four stations to determine the temperature distribution over the model surface. To avoid viewing the radiation from the hot shock layer, the models are made to pass through helium over a distance of about 1.5 m while the photograph is taken. This is accomplished by flushing the test gas in front of the camera with helium starting immediately before the arrival of the model, as mentioned earlier.[6]

Radiative Transfer

The CMA code requires wall radiative and convective heat-transfer rates as inputs. The radiative heat fluxes emanating from an inviscid argon shock layer over a 5.08-cm-diam flat disk have been calculated in Ref. 9. The calculating method is first compared with that used in RASLE.[11] The version of RASLE used in the comparison contains spectral data of argon that are provided by W. E. Nicolet, Thermal Sciences, Inc., Sunnyvale, Calif., and A. Balakrishnan of PEDA Corporation, Palo Alto, Calif. The comparison reveals that at the edge of the ablation layer, taken here to be the inner 30%

Table 1 Test conditions

	Shot number					
Launch conditions	5591	5599	5601	5602	5604	5605
Material	CC	CMCP	CMCP	CMCP	ICCP	CC
p_∞, Torr	50	50	50	25	50	75
Initial v_∞, km/s	5.465	5.419	5.483	5.364	5.410	5.364
Final v_∞, km/s	4.923	4.858	4.902	5.059	4.830	4.566
Initial p_s, atm	31.5	30.9	31.7	15.2	30.8	45.6
Final p_s, atm	25.6	24.9	25.3	13.5	24.6	32.9
Initial Mach No.	17.0	16.8	17.0	16.7	16.8	16.7
Initial $Re \times 10^{-6}$	2.54	2.51	2.55	1.25	2.51	3.70
$\int_0^\infty q_{cw} dt$, KJ/cm^2	0.019[a]	0.075[b]	0.070[b]	—	0.066[b]	0.020[a]
$\int_0^\infty q_{rw} dt$, KJ/cm^2	1.69[a]	1.15[b]	1.18[b]	—	1.14[b]	1.77[a]
Model recovery	Yes	Yes	Yes	No	Yes	Yes

[a] SPAIFT. [b] Coupled boundary-layer/radiation/CMA code.

of the overall shock-layer thickness, the radiative heat fluxes calculated by the two methods are nearly identical. These flux values, denoted q_A, are "blocked" by the ablation layer. The wall radiative heat flux is expressed by multiplying q_A by a "radiative blockage factor" ϕ.

$$\text{wall radiative heat flux} = q_{rw} = \phi q_A \tag{1}$$

To determine the radiative blockage factor, transfer of the radiation power emanating from the inviscid region and passing through the ablation layer is calculated. The ablation-layer profiles are obtained by the method described later (see subsection on boundary-layer analysis). The radiative transfer calculation is performed using the technique described in Ref. 13 including all seven band systems of C_2 (see Ref. 13) and the C_3 continuum in the ultraviolet wavelength range.[14,15] These calculations are carried out for three different ablation rates (see subsection on recession calculation) for each flight. The resulting values of ϕ are fitted by

$$\phi = \exp(a_1 + a_2 |f_w| + a_3 |f_w|^2) \tag{2}$$

where f_w is the wall value of the dimensionless velocity function in the boundary-layer coordinate system which is related to the ablation rate $\dot{m}$ by[16]

$$\dot{m} = \Phi |f_w| \tag{3}$$

where

$$\Phi \equiv 2^{0.75} (\rho_e/\rho_\infty)^{0.25} (\mu_e/\mu_\infty)^{0.5} \rho_\infty v_\infty / (Re_\infty)^{0.5} \tag{4}$$

Here ρ and μ are density and viscosity, respectively, and Re_∞ is the freestream Reynolds number $Re_\infty = \rho_\infty v_\infty R_n / \mu_\infty$; where v_∞ and R_n are the freestream velocity and the equivalent sphere radius, respectively. R_n is determined using the formula given in Ref. 9. The subscripts e and ∞ refer to the edge of the ablation layer and the freestream, respectively. The three-parameter expression, Eq. (2), is believed to be adequately accurate in the present work because ablation rate $\dot{m}$, and hence f_w, varies over a narrow range (see subsection on general features of the solutions). Viscosity is approximated by

$$\mu = 2.22 \times 10^{-4} (T/300)^{0.8} \text{poise}, \quad \text{for } 300\text{ K} < T < 5000\text{ K} \tag{5}$$

$$\mu = 2.11 \times 10^{-3} \text{poise}, \quad \text{for } 5000\text{ K} < T \tag{6}$$

The expression is accurate for argon at 300 K, and approximates the viscosity of ionized argon within ±30% (see Ref. 17). In addition, the expression reproduces the viscosity values predicted for the ablation-product gases from carbonaceous heat shields[18] to within about 25%.

Boundary-Layer Analysis

As mentioned earlier, two different types of convection phenomena occur in the present problem: the regular boundary-layer type ablation while the model passes through argon, and the nearly explosive ablation occurring while the model passes through helium. The boundary-layer flow is solved for the regular ablation environment in order to provide the flow property profiles needed for the radiative transfer calculation. The duration over which the nearly explosive ablation occurs is short, and hence the phenomenon can be ignored for the recession calculation (see subsection on general features of the solutions). The boundary-layer characteristics in the stagnation region of a flat disk are the same as those of a sphere producing the same pressure gradient, that is, a sphere of equivalent nose radius R_n.

In the regular ablating environment, relative diffusion among the different species in the gas is slow compared with the bulk velocity of the mixture because of the massive-blowing nature. The ablation-product gas can be considered, therefore, to move as a bulk, as if it were a single species. Denoting the mass fraction of the ablation-product species by α, therefore, the rate of its production must satisfy a global Knudsen-Langmuir equation[19]

$$\dot{m} = \beta \rho_w C_w (\alpha_{Ew} - \alpha_w)/4 \tag{7}$$

where β and C_w are vaporization coefficient and mean molecular speed of the ablation-product species at wall temperature, respectively; the subscript E denotes equilibrium. The vaporization coefficient β is varied between 0.1 and 1; little difference is seen in the results.

The equilibrium wall mass fraction α_{Ew} is calculated from the equilibrium vapor pressure p_E and the mean molecular weight, which are dictated by the thermochemistry of the ablation-product gases and, for carbon-phenolic, by the ratio of pyrolysis-gas to char-gas flow rates. The thermochemical data used by Moss and Simmonds[20] are adopted in the present work. The pyrolysis-to-char gas flow ratio is taken to be 0.267, which is a best-fitting mean value in the present environment. Using the computer code ablating chemical equilibrium (ACE),[21] p_E is found to be expressible as

$$p_E = 6.27 \times 10^{15} \exp(-90908/T_w) \text{ dyne/cm}^2$$

for carbon-phenolic and as

$$p_E = 5.19 \times 10^{15} \exp(-90845/T_w) \text{ dyne/cm}^2$$

for carbon-carbon. The average molecular weight is found also from the ACE code to be 35 ±1 for both carbon-phenolic and carbon-carbon in the range of interest.

The wall-mass fraction α_w appearing in Eq. (7) is determined by solving the system of boundary-layer equations. Under the present assumption, the species satisfies the equations of a frozen flow, since the freestream gas (argon) is inert. After the well-known coordinate transformation, the mass, momentum, and energy conservation equations for the boundary layer over the stagnation point reduce to three simultaneous ordinary differential equations.[16,22] The boundary conditions for the frozen boundary layer are also well known.[16,22]

These differential equations are integrated numerically for the three selected ablation rates mentioned earlier to determine $\dot{m}$ and f_w for the three conditions. The Prandtl and Schmidt numbers are assumed to be

$$Pr = 0.4(T_w/T) \tag{8}$$

$$Sc = 0.5(T_w/T) \tag{9}$$

The quantity $\rho\mu$ is assumed to be inversely proportional to temperature to be consistent with Eq. (6). The temperature variation within the boundary layer is approximated in turn by a relationship similar to that used in Ref. 22. The transport properties so chosen roughly recreate those obtained using a rigorous method[11] (see subsection on general features of the solutions).

The right-hand side of the energy equation representing energy addition by radiation absorption is calculated through an iterative procedure: it is first assumed to be zero. From the resulting profiles of energy and mass fraction of the ablation-product gas, the temperature and concentration of various gas species are determined by invoking the equilibrium relationship.[24] The radiative transfer calculation is then carried out using the method of Ref. 13 to obtain the energy addition to a unit volume. The ablation layer is divided into nine isothermal layers of unequal thicknesses (thinner toward wall) for this purpose. The second approximation to the energy equation is then obtained by integrating the system of equations accounting for the finite right-hand side. The third approximation is adopted as the final solution. A discrepancy

of less than 0.5% was seen between the wall heat flux values of the third and the second approximations.

Recession Calculation

For the purpose of determining surface recession, the three constants a_1, a_2, and a_3 specifying the radiative blockage factor are first calculated. For each test, the time-velocity-distance record is available as basic test data. For the calculation of a_i, the inviscid layer conditions are fixed at those occurring at the midpoint of the uprange. The radiation spectra incident on the edge of the ablation layer are obtained by carrying out the radiative transfer calculation for an inviscid shock layer.[9] The boundary-layer calculation and radiative transfer calculation described in the preceding subsections are then made for three arbitrarily chosen ablation rates. By dividing the resulting wall radiative heat flux values by the edge value, the radiative blockage factors for the three ablation rates are determined. By curve fitting the blockage factor values with Eq. (2), the constants a_i are obtained.

The standard CMA code is modified so as to accept radiative and convective heat-transfer rates as a function of the ablation rate. At any given time instant, the radiative heat flux incident on the edge of the ablation layer q_A is calculable by interpolating the results of the radiation calculation for an inviscid shock layer.[9] By multiplying q_A by ϕ obtained using the constants a_1, a_2, and a_3, the wall radiative heat flux q_w is obtained. The convective heat-transfer rate is calculated by multiplying the zero-ablation value of Fay and Riddell[22] by the blowing-correction factor given by Putz and Bartlett.[23] With the radiative and convective heat-transfer rates so specified, the CMA code computes conduction and pyrolysis in the material and surface recession.

The CMA code requires material properties as additional inputs. The density ρ_m of carbon-phenolic is given in Ref. 25 as 1.446 g/cm^3 in the virgin state, and 1.191 g/cm^3 in the char state. Carbon-phenolic is assumed to consist of 92.36% carbon, 2.09% hydrogen, and 5.55% oxygen by weight. The density of the carbon-carbon composite material used here is determined to be 1.74 g/cm^3. Specific heat values of carbon-phenolic given in Ref. 25 vary from 0.962 J/g-K at room temperature to 2.30 J/g-K at 3333 K for the virgin material, and from 0.703 to 1.88 J/g-K for the char. The specific heat of carbon-carbon is taken to be the same as that of graphitic carbon.[26]

The thermal conductivity values used in the calculation are shown in Fig. 1. The solid curves in the figure represent the available experimental data, and the dashed curves show how the experimental data are extended to higher temperatures in the present work. The experimental data for carbon-carbon are supplied by Science Applications, Inc. (SAI), and are unpublished. As the figure shows, the experimental data are available for temperatures only up to about 2300 K. The values are assumed to decrease beyond 2300 K, following the general trend of graphites.[26] Two sets of experimental data exist for carbon-phenolic; those given by Bueche of General Electric Co.,[25] which will be referred to hereafter as GE conductivities, and those by Wakefield and Pitts[27] of Ames Research Center, which will be called the Ames values. For the GE values, conductivity values are extrapolated by a straight line to higher temperatures. Extrapolation of the Ames data is made by compromising between the increasing trend of the experimental data and the generally decreasing trend of the conductivity values for graphites.[26] Calculations for carbon-phenolic are carried out using both sets of conductivity values. Time integration is extended 1 s beyond the end of the model flight in order to allow for temperature redistribution within the solid.

Nearly Explosive Mass Transfer in Helium

While the model passes through helium in front of an imacon camera, a nearly explosive mass transfer occurs. Since

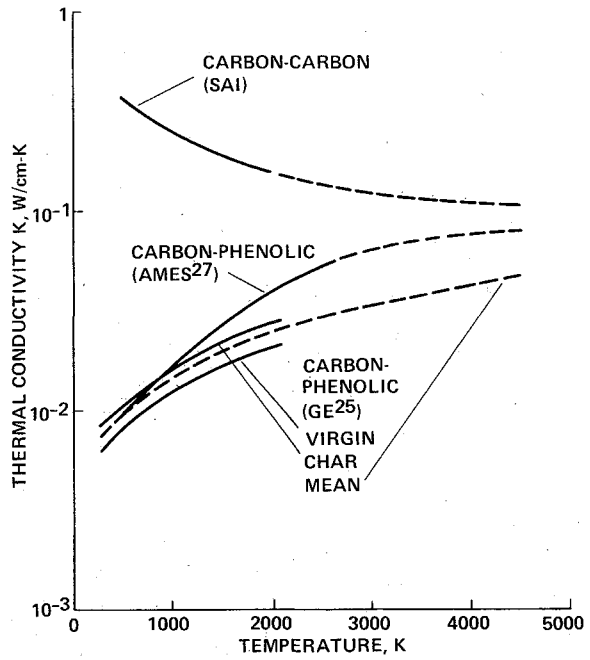

Fig. 1 Thermal conductivities of carbon-phenolic and carbon-carbon heat-shield materials.

duration of this flight is short, it affects overall surface recession to a negligible extent. However, the process must be calculated in order to properly interpret the ima-con photographs of the frontal surface of the models.

As the model enters the helium region, the stagnation pressure p_s becomes momentarily lower than the equilibrium vapor pressure p_E. Hence, the ablation-product gas expands adiabatically. The ablation rate can be expressed by the Knudsen-Langmuir equation in the form[19]

$$\dot{m}=\beta C_w m(p_E-p_w)/(4kT_w) \tag{10}$$

where m and k are the mean molecular mass and Boltzmann constant, respectively. The wall pressure p_w in Eq. (10) obeys the following one-dimensional gasdynamic equations:

$$\rho v=\text{const} \tag{11}$$

$$v\frac{\mathrm{d}v}{\mathrm{d}y}=-\frac{1}{\rho}\frac{\mathrm{d}p}{\mathrm{d}y} \tag{12}$$

$$p/\rho^{\gamma}=\text{const} \tag{13}$$

Here y is the distance from the wall. The adiabatic exponent γ is assumed to be 1.2. The boundary conditions are $p=p_w$ at $y=0$, and $p=p_s$ at $y=\infty$. On integrating these equations, and eliminating all variables except pressure, the wall mass balance condition becomes

$$[(p_E/p_w-1)(\beta/4)]^2[(p_w/p_s)^2-1]\rho_w C_w^2/p_w - [\gamma/(\gamma-1)][1-(p_s/p_w)^{(\gamma-1)/\gamma}]=0 \tag{14}$$

Equation (14) is solved numerically. While the nearly explosive ablation is occurring, both the radiative and convective heat-transfer rates are zero. Even so, the surface cools rapidly, mainly due to the fast sublimation [Eq. (10)].

To compute the surface temperature as a function of time, one must integrate conduction and pyrolysis rate equations. The CMA code is unsuitable for this purpose because it does not allow for the nearly explosive mass-transfer phenomenon. Hence, an approximate calculation is made neglecting pyrolysis, that is, by assuming that solid-to-gas conversion

occurs at the wall surface only. The energy transfer through the solid then occurs only in the conduction mode, which is represented by

$$\rho_m C_{pm}\left(\frac{\partial T}{\partial t}+V\frac{\partial T}{\partial y}\right)=\frac{\partial}{\partial y}\left(K\frac{\partial T}{\partial y}\right) \tag{15}$$

where C_p and K are specific heat and thermal conductivity, respectively, and V is the recession velocity $V=-\dot{m}/\rho_m$. For numerical computation, Eq. (15) is written in a difference form in y, employing a central difference scheme. A total of 32 equally spaced nodal points is taken in the y direction. The temperature of the 32nd node is assumed to be at room temperature. At the wall, the rate of heat input is given by

$$q_a=e\phi q_A+q_{cw}-e\sigma T_w^4-h_v\dot{m} \tag{16}$$

where e, σ, and h_v are surface emissivity, Stefan-Boltzmann constant, and heat of vaporization, respectively. The quantity q_{cw} is the convective heat-transfer rate obtained by multiplying the value of Fay and Riddell[22] by the convective shielding factor of Putz and Bartlett.[23] The vaporization energy h_v is determined using the ACE code to be 31,000 J/g for carbon-carbon, and 30,000 J/g for carbon-phenolic in the range of pressure and temperature of interest. While the model passes through argon, that is, in the regular ablating region, the ablation rate $\dot{m}$ is determined by assuming that the convective shielding factor of Putz and Bartlett[23] for heat conduction applies also for mass transfer. For carbon-phenolic, the averages between the virgin and shear values are used for the effective thermal conductivity and specific heat (see Fig. 1).

The difference form of Eq. (15) becomes a set of 31 simultaneous ordinary differential equations with time t as the independent variable and 31 temperature values as dependent variables. The system is integrated using the second-order implicit integrating scheme of Lomax.[28] The calculation is carried out with a code to be identified as stagnation point ablation in flight test (SPAIFT).

Results

General Features of the Solutions

Figure 2 compares the computed temperature profiles and the profiles of C_2 and C_3 concentrations with those obtained by RASLE.[11] as seen here, the two temperature profiles are nearly identical. The species concentration profiles differ slightly, but their integrated values are also nearly the same. For the case shown, the present calculation results in a radiative blockage factor of 0.57 as compared to 0.59 by RASLE. Hence, one concludes that the present boundary-layer approach reproduces the results of the viscous shock-layer method used in RASLE for the conditions of interest.

Time histories of absorbed heat flux q_a [see Eq. (16)], wall temperature T_w, mass-loss rate $\dot{m}$, and blowing parameter $B'=\dot{m}/(\rho_\infty v_\infty C_h)$ calculated using the SPAIFT code are shown in Figs. 3-6 for one carbon-carbon (shot 5591) and one carbon-phenolic (shot 5601) model. The results shown are obtained using the Ames conductivity values (see Fig. 1). The highest heat-transfer rates occur at $t=0$ (see Fig. 3) because flight velocity is the highest and because there is no ablation layer to cause radiative or convective blockage. The wall heat flux decreases as the ablation layer develops. Eventually, the stagnation-point wall temperature reaches a value only slightly below the equilibrium temperature corresponding to the prevailing stagnation pressure. For shots 5591 and 5601, the peak wall temperatures are 4740 K and 4670 K, respectively. The corresponding mass-loss rates are 0.41 and 0.68 g/cm^2-s. When the model enters the helium region in front of an ima-con camera, the mass-loss rate becomes very large because the equilibrium vapor pressure is greater than the shock-layer pressure, leading to a nearly free evaporation

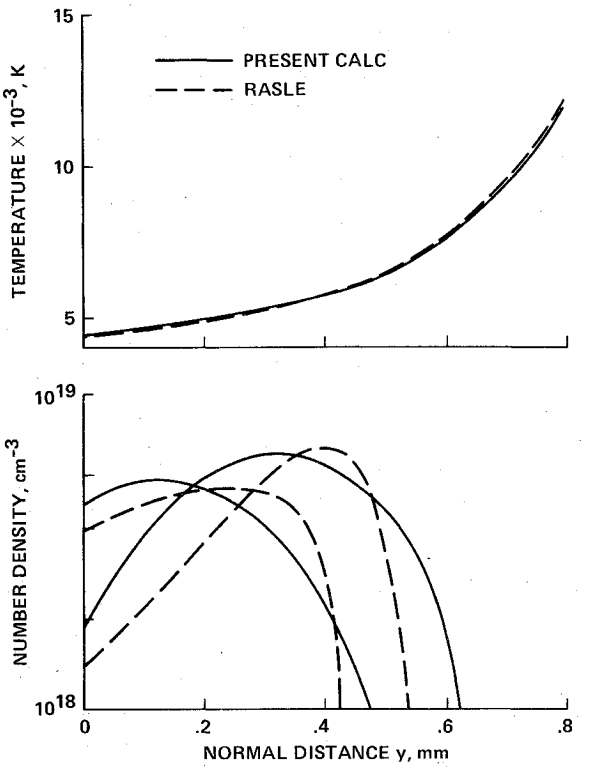

Fig. 2 Comparison of temperature and C_2 and C_3 number densities for the boundary-layer solution and the RASLE solution.

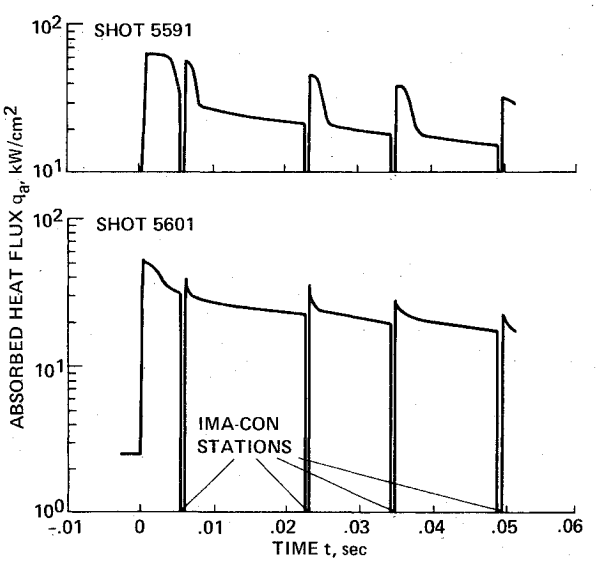

Fig. 3 Typical time histories of absorbed heat flux (SPAIFT calculation).

resembling an explosion (Fig. 5). Wall heat flux plunges to zero because there is neither radiative nor convective heat transfer. The rapid vaporization causes a correspondingly rapid cooling of the wall surface. When the equilibrium vapor pressure falls below the shock-layer pressure, convective cooling by relatively cold (about 3000 K) helium begins. The cooling ceases when the wall temperature nearly equals the helium shock-layer temperature. The minimum temperature occurring at the ima-con stations (see Fig. 4) are close (to within 20 K) to the helium shock-layer temperature. As the model re-enters the argon region, heating and regular ablation resume. The blowing parameter B' reaches nearly 40 for the carbon-carbon and 350 for the carbon-phenolic models, demonstrating that the flows are in a massive-blowing regime.

In order to assess the contribution of the nearly explosive ablation and subsequent cooling to the overall recession, the

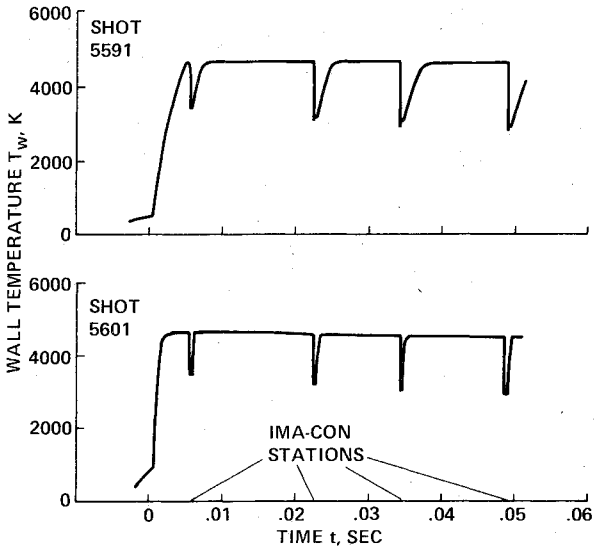

Fig. 4 Typical time histories of wall temperature (SPAIFT calculation).

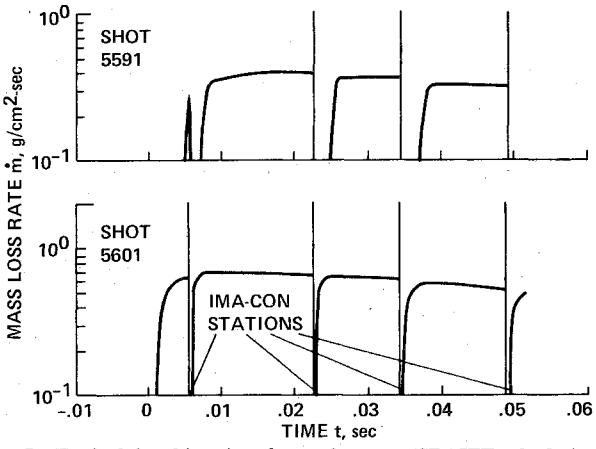

Fig. 5 Typical time histories of mass-loss rate (SPAIFT calculation).

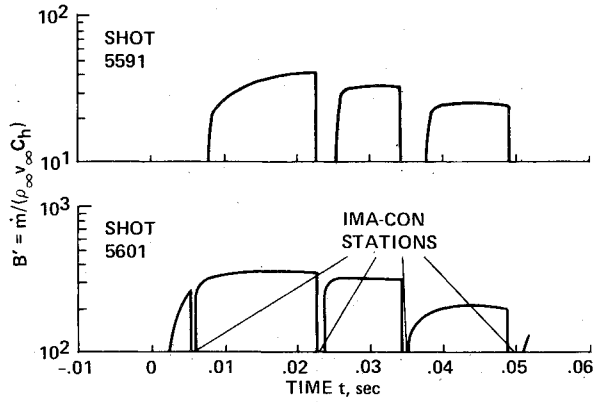

Fig. 6 Typical time histories of blowing parameter $B' = \dot{m}/(\rho_\infty v_\infty C_h)$ (SPAIFT calculation).

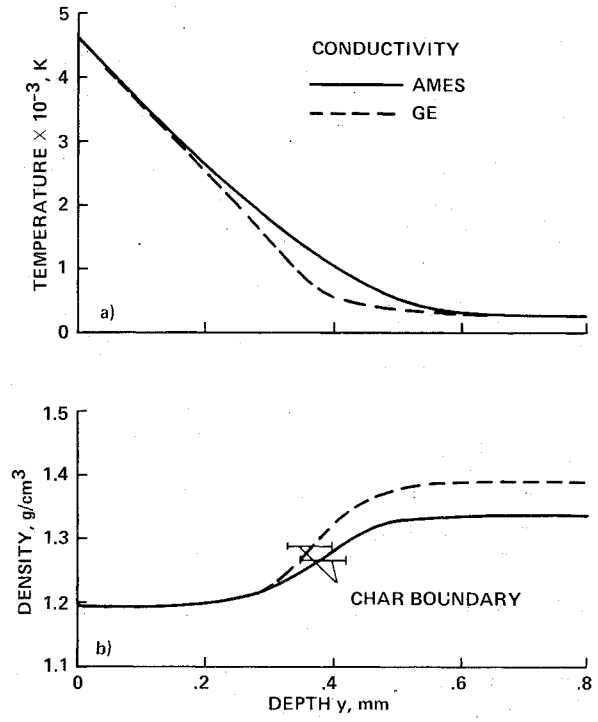

Fig. 7 Results of CMA calculation for shot 5601 obtained using the thermal conductivity values of GE[25] and Ames[27]: a) temperature profiles at the end of flight, b) density profile at $t = 1$ s.

SPAIFT calculation is repeated without the helium region. The resulting overall recessions are found to be slightly greater, that is, by less than 5%. For the purpose of calculating surface recession, therefore, the nearly explosive phenomenon need not be considered.

Recession and Char Thickness

The coupled boundary-layer/radiation/CMA calculation resulted in temperature and ablation rate histories closely resembling those obtained by the SPAIFT calculation, except that the nearly explosive ablation and the subsequent rapid cooling in the ima-con stations are absent (because they are not accounted for). The wall temperature and ablation rates computed by the coupled boundary-layer/radiation/CMA code lag slightly behind those of the SPAIFT calculation, understandably due to the initial transient in which heat is absorbed for the in-depth pyrolysis reactions. Surface recessions continue for a short while beyond the flight end points.

Figure 7a compares the temperature distributions within carbon-phenolic at the end of the flight determined using the two different conductivity values. There is only a small difference in the two temperature profiles. Distributions of density at the end of a 1-s period calculated using the two conductivity values are shown in Fig. 7b. As seen here, density changes from the virgin to the char value over a relatively narrow region. The midpoints of the density change are referred to in the figure as the char boundary. If a tested model were sliced and split to reveal its cross sections, the density change would appear as a change in texture and color (from light to dark gray). The color change should occur most rapidly at the midpoint of the density. The horizontal error bars around the boundary points in the figure indicate the possible ranges of uncertainty in the visual determination of the boundary point on the split model, and correspond to the ¼- and ¾-density change points. As seen in the figure, the range of uncertainty in determining the thickness of a char is likely to be about ±12%. There is little difference in char thickness between the two conductivity values.

Table 2 lists the surface recessions and char thicknesses computed by the CMA method using the different conductivity values. Again, there is virtually no difference seen between the results obtained using the two sets of conductivity values. The calculated surface recessions and char thicknesses vary from about 0.08 to 0.18 mm and from 0.37 to 0.39 mm, respectively. These recession values are sufficiently large to be experimentally verified. Although not indicated in the table,

Table 2 Surface recession δ and char thickness Δ for five recovered models,[a] calculated with different conductivity *K*, using the combined boundary-layer/radiation/CMA code

Case	Shot	Material	*K*	δ, mm	Δ, mm
1	5591	CC	SAI	0.0904	
2					
3	5599	CMCP	Ames	0.174	0.385
4			GE	0.179	0.378
5	5601	CMCP	Ames	0.182	0.378
6			GE	0.186	0.370
7	5604	ICCP	Ames	0.172	0.387
8			GE	0.175	0.380
9	5605	CC	SAI	0.111	

[a] δ and Δ were not calculated for shot 5602; the model was lost during recovery.

these recession values are about 15% smaller than those calculated by the SPAIFT code. The difference can be attributed to the pyrolysis phenomenon neglected in the SPAIFT calculation.

Conclusions

Flat disks (5 cm diameter) launched in the Track-G facility of AEDC into ambient argon at around 50 Torr are subject to radiative wall heating of a few tens of kW/cm^2. Blowing parameters of the order of 100 and Reynolds numbers greater than 10^6 are produced at hypersonic Mach numbers by this means. For carbon-carbon and carbon-phenolic models, the theory predicts recessions of approximately 0.1 and 0.18 mm, respectively. Char thickness for the carbon-phenolic models becomes approximately 0.38 mm. The conductivity values given by General Electric Co. and those given by Ames Research Center result in nearly identical recessions and char thicknesses. Temperature of the wall becomes approximately 3000 K while the models pass through helium.

Acknowledgments

The author wishes to express his sincere thanks to W. E. Nicolet of Thermal Sciences, Inc., Sunnyvale, Calif. and A. Balakrishnan of PEDA Corporation, Palo Alto, Calif., for providing the spectral data for argon for use in the RASLE code, and for their assistance in running the RASLE code.

References

[1] Lees, L., "Convective Heat Transfer with Mass Addition and Chemical Reactions," *Combustion and Propulsion*, 3rd AGARD Colloquium, Pergamon Press, New York, 1959, pp. 451-498.

[2] Nicolet, W. E., Vojvodich, N. S., and Morse, H. L., "Outer Planet Probe Entry Thermal Protection. Part 1. Aerothermodynamic Environment," AIAA Paper 74-700, Boston, Mass., July 1974.

[3] Park, C. and Bowen, S. W., "Ablation and Deceleration of Mass-Driver Launched Projectiles for Space Disposal of Nuclear Wastes," Progress in Astronautics and Aeronautics, *Thermophysics of Atmospheric Entry*, Vol. 82, edited by T. E. Horton, AIAA, New York, N.Y, 1982, pp. 201-225.

[4] Nicolet, W. E., Howe, J. T., and Mezines, S. A., "Outer Planet Probe Entry Thermal Protection. Part 2. Heat Shielding Requirements," AIAA Paper 74-701, Boston, Mass., July 1974.

[5] Howe, J. T., Pitts, W. C., and Lundell, J. H., "Survey of the Supporting Research and Technology for Thermal Protection of the Galileo Probe," AIAA Paper 81-1068, Palo Alto, Calif., June 1981.

[6] Norfleet, G. D., Hendrix, R. E., Raper, R. M., and Callens, E. E. Jr., "Development of an Aeroballistic Range Capability for Testing Reentry Materials," *Journal of Spacecraft and Rockets*, Vol. 12, May 1975, pp. 302-307.

[7] Miller, J. T., "Aeroballistic Range Tests of Ablating Heat Shield Materials—Interim Report," Arnold Engineering Development Center, Arnold Air Force Station, Tenn., AEDC-TR-70-114, May 1970.

[8] Miller, J. T. and Raper, R. M., "Aeroballistic Range Tests of Ablating Heat Shield Materials—Final Report," Arnold Engineering Development Center, Arnold Air Force Station, Tenn., AEDC-TR-70-285, Jan. 1971.

[9] Park, C., "Calculation of Radiation from Argon Shock Layers," *Journal of Quantitative Spectroscopy and Radiative Transfer*, Vol. 28, No. 1, July 1982, pp. 29-40.

[10] Park, C., "Ablation of Carbonaceous Flat Disks in Argon-Filled Ballistic Range. Part 2. Experiment," accepted for publication in *AIAA Journal*.

[11] Nicolet, W. E., "Radiation Heating Environments for Jovian Entry Conditions," Progress in Astronautics and Aeronautics, *Radiative Transfer and Thermal Control*, Vol. 49, edited by A. M. Smith, AIAA, New York, 1976, pp. 231-250.

[12] Kendall, R. M., Rindal, R. A., and Bartlett, E. P., "Thermochemical Ablation," AIAA Paper 65-642, Monterey, Calif., Sept. 1965.

[13] Arnold, J. O., Cooper, D. M., Park, C., and Prakash, S. G., "Line-by-Line Transport Calculations for Jupiter Entry Probes," Progress in Astronautics and Aeronautics, *Entry Heating and Thermal Protection*, Vol. 60, edited by W. B. Olstad, AIAA, New York, N.Y., 1980, pp. 52-82.

[14] Prakash, S. G. and Park, C., "Shock Tube Spectroscopy of $C_3 + C_2H$ Mixture in the 140-700 nm Range," AIAA Paper 79-0094, New Orleans, La., Jan. 1979.

[15] Shinn, J. L., "Optical Absorption of Carbon and Hydrocarbon Species from Shock Heated Acetylene and Methane in the 135-220 nm Wavelength Range," AIAA Paper 81-1189, Palo Alto, Calif., June 1981.

[16] Dorrance, W. H., *Viscous Hypersonic Flow*, McGraw-Hill, New York, N.Y., 1962, pp. 29-30, 45-56, and 79-88.

[17] Gopalakrishna, K., "High Temperature Transport Properties of Argon Plasma," Harvard University, Cambridge, Mass., Engineering Science Laboratory Rept. TR-29, March 1967.

[18] Amarly, B. F. and Sutton, K., "Viscosity of Multicomponent Partially Ionized Gas Mixtures," AIAA Paper 80-1495, Snowmass, Colo., July 1980.

[19] Hirth, J. P. and Pound, G. M., *Condensation and Evaporation*, Pergamon Press, Oxford, United Kingdom, 1963, p. 2.

[20] Moss, J. N. and Simmonds, A. L., "Galileo Probe Forebody Flowfield Predictions During Jupiter Entry," AIAA Paper 82-0874, St. Louis, Mo., June 1982.

[21] Powers, C. A. and Kendall, R. M., "User's Manual, Aerotherm Chemical Equilibrium (ACE) Computer Program," Aerotherm Corp., Mountain View, Calif., May 1969.

[22] Fay, J. A. and Riddell, F. R., "Theory of Stagnation Point Heat Transfer in Dissociated Air," *Journal of the Aeronautical Sciences*, Vol. 25, No. 2, Feb. 1958, pp. 73-97.

[23] Putz, K. E. and Bartlett, E. P., "Heat-Transfer and Ablation-Rate Correlations for Re-Entry Heat-Shield and Nosetip Applications," *Journal of Spacecraft and Rockets*, Vol. 10, Jan. 1973, pp. 15-22.

[24] Perini, L. L., "Curve Fits of JANAF Thermochemical Data," Johns Hopkins University, Baltimore, Md., Applied Physics Laboratory Report ANSP-M-5, Sept. 1972.

[25] Bueche, J. F., "Effects of Improvements and Uncertainties in Thermophysical Properties on Carbon-Phenolic Heat Shield Thermal Performance Predictions," AIAA Paper 77-787, Albuquerque, N. Mex., June 1977.

[26] Touloukian, Y. S., *Thermophysical Properties of High Temperature Solid Materials, Vol. 1. Elements*, Macmillan Co., New York, N.Y., 1967, pp. 83-391.

[27] Wakefield, R. M. and Pitts, W. C., "Analysis of the Heat-Shield Experiment on the Pioneer-Venus Entry Probes," AIAA Paper 80-1494, Snowmass, Colo., July 1980.

[28] Lomax, H., "Stable Implicit and Explicit Numerical Methods for Integrating Quasi-Linear Differential Equations with Parasitic-Stiff and Parasitic-Saddle Eigenvalues," NASA TN D-4703, 1968.